11th ANKARA INTERNATIONAL AEROSPACE CONFERENCE **AIAC-2021-079**
8-10 September 2021 - METU, Ankara TURKEY

DETERMINATION OF WAKE SHAPES BEHIND A WIND TURBINE THROUGH CFD SIMULATIONS AND COMPARISON WITH ANALYTICAL WAKE MODELS

Ali Ata Adam*
METU
Ankara, Turkey

Olcay Nurtaç Deniz†
Turkish Aerospace
Ankara, Turkey
METU
Ankara, Turkey

Nilay Sezer-Uzol‡
METU
Ankara, Turkey

Oğuz Uzol§
METU
Ankara, Turkey

ABSTRACT

In this paper, wake shapes of wind turbine rotors are investigated by using CFD and analytical wake models. The flow around the NTNU model turbine is simulated using the Reynolds-Averaged Navier-Stokes Equations with Spalart-Allmaras, standard $k-\epsilon$, standard $k-\omega$, and $k-\omega$ SST turbulence models, $k-k_L-\omega$ and Transition SST transition models and also with two different freestream turbulence intensities as low and high values of 0.23% and 10%, respectively. The simulations are done for a single turbine and then for two aligned turbines, one behind another. The wake velocity profile results obtained from the CFD simulations at different downstream locations are compared with the available experimental measurements and with the calculated analytical wake model results and also among each other. The results show that CFD tools are necessary to investigate the unsymmetrical wake shape near the rotor. However, the wake models may predict the average flow speed away from the turbine well. Moreover, the models developed with detailed methods can predict the velocity profiles much better in shape, especially when there is a high turbulence level in the flow. Moreover, the two-turbine case results from the wake models show that the wake superposition method could significantly impact the velocity distribution within a wind farm.

INTRODUCTION

There has been a tremendous rise in wind energy production, especially after the late 1980s [Our World In Data, 2021; BP, 2021] boosted by the oil crises in the past [Vermeer et al., 2003; Saidur et al., 2010], global climate change [Sahin, 2004], and plummeted cost in wind energy production [Lantz et al., 2012]. However, there is only limited land where the wind energy potential is plentiful.

*Graduate Research Assistant, Dept. of Aerospace Engineering. Email: adam@metu.edu.tr
†Aerodynamics Design Engineer, Turkish Aerospace Industries Inc.. Graduate Student, Dept. of Aerospace Engineering, Middle East Technical University. Email: olcay.deniz@metu.edu.tr
‡Assoc. Prof. Dr., Dept. of Aerospace Engineering. Email: nuzol@metu.edu.tr
§Prof. Dr., Dept. of Aerospace Engineering. Email: uzol@metu.edu.tr

Moreover, the array efficiency in a wind farm, an indicator of farm layout efficiency, depends on many variables and must be maximized to extract the most energy possible [Milborrow, 1980]. Depending on the oncoming wind characteristics, the turbine rotors and wake flow fields interact with each other affecting the power outputs and efficiency of the wind farms. Thus, wind turbines may be placed in different layouts to maximize the energy output in the wind farm. As wind farm simulations require extensive computational resources to simulate these complex flow interactions, analytical and empirical modeling approaches have been developed for wake modeling. Wind farm layout modeling and optimization studies mainly focused on more accurate wind turbine wake predictions, wind turbine rotor modeling with actuator disk or actuator line methods, topography analysis, and thus computational cost reduction. Getting more power from a wind farm, thus increasing the annual energy production, can be achieved with more realistic models and less computational cost, providing accurate and efficient power predictions for wind farm control, turbine design, or both.

In recent years, there have been several experimental and computational studies on the investigation of wind turbine rotor wake in the literature. Although there are not many studies on field measurements, such papers remarkably reveal the actual flow conditions in a wind farm. Researchers usually utilize volumetric light detection and ranging (LiDAR) measurements of the turbine wakes and analyze the flow data they obtain [El-Asha et al., 2017; Torres Garcia et al., 2019]. Moreover, the power produced by the turbines and meteorological data measured by met-towers are valuable parameters in this topic [El-Asha et al., 2017]. These field measurements showed that convective atmospheric conditions might cause the wakes to recover much more quickly. Thus, the power loss of a single turbine could be one-third of that in stable atmospheric conditions [El-Asha et al., 2017]. Although the wake center lines align with the wind direction in most cases, the interactions between the rotor wakes could cause them to be misaligned [Torres Garcia et al., 2019]. In addition, the limited streamwise spacing between the turbines could cause greater power losses due to the measured significant adverse waked conditions within the wind farm [El-Asha et al., 2017].

The measurements from the actual wind farms showed that there would be a great need for the understanding of wind turbine wakes and their interactions with numerous variables. Thus, many wind tunnel experiments have been conducted on the subject. Researchers could investigate the wake characteristics in terms of the studied variables since these parameters can be controlled in a wind tunnel much easier compared to a real wind farm. Wind turbines can easily be positioned within the wind tunnel to observe the effect of wind farm layout. Such configurations could be in tandem [Adaramola and Krogstad, 2011; Bartl et al., 2012; Schümann et al., 2013; Pierella and Sætran, 2017] or yawed [Adaramola and Krogstad, 2011]. Thus, the power dependence on the yaw angle of the rotors, the layout, or the rotational speed of turbines could be assessed [Adaramola and Krogstad, 2011]. Besides, the wake shapes behind the turbines can be measured by the hot-wire or n-hole probes, as well as particle visualization techniques like PIV or LDA [Bartl et al., 2012; Schümann et al., 2013; Pierella and Sætran, 2017]. The experiments on the wake characteristics have shown that the wake behind a turbine operating under the wake of the upstream turbine is similar to the one behind a turbine operating under a clean wind. It has an asymmetrical velocity profile near the turbine due to the tower wake as in the upstream wake profile [Pierella and Sætran, 2017]. Nevertheless, its velocity deficit is much higher because the turbine operates under a lower velocity than the upstream turbine [Bartl et al., 2012]. In addition, due to the higher turbulence intensity, the wake behind the downstream turbine recovers more quickly [Schümann et al., 2013; Pierella and Sætran, 2017] and becomes more symmetrical and uniform compared to the upstream wake [Bartl et al., 2012].

The complexity in wind turbine wakes brings multiple alternative settings for the computational simulations. The results from the NTNU Blind Test Workshops held between 2011 and 2017 [Krogstad and Eriksen, 2013; Pierella et al., 2014; Krogstad et al., 2015; Bartl and Sætran, 2017; Mühle et al., 2018] have shown significant differences between the numerical results obtained with different flow solvers and turbulence models. NTNU model turbine was simulated by using many different solver types, including the BEM method, panel method, RANS and LES based in-house, commercial, and

open-source CFD flow solvers, and with various turbulence models ranging from Spalart-Allmaras to $k-\omega$ SST. Moreover, the modeling of the turbine components and wakes are crucial aspects of the simulations. Although the workshop findings showed that Large Eddy Simulation (LES) should be the most probable selection for solving the flow within the wind farm due to the complex interactions between turbines and wakes, it comes with a high computational price for such a compound configuration. Thus, many studies sought the answer to the question of whether Reynolds-Averaged Navier-Stokes (RANS) equations can be implemented without losing significant accuracy or not. Such studies implemented RANS equations with many different turbulence models and many of them successfully validated the simulation results with the available wind farm data. Eddy-viscosity-based models like $k-\epsilon$ [Avila et al., 2013; Kuo et al., 2016; Antonini et al., 2019; Richmond et al., 2019; Behrouzifar and Darbandi, 2019], $k-\omega$ [Antonini et al., 2019], and $k-\omega$ SST [Antonini et al., 2019; Richmond et al., 2019; Antonini et al., 2020], and Reynolds Stress models [Antonini et al., 2019] can be given as examples to the validated models.

Although modeling the turbine as it is in the simulations gives the most accurate results, this choice may bring an unpractical computational cost because of the high complexity in the wind farm simulations. Therefore, it is seen that actuator disk models can be implemented for turbine blades [Avila et al., 2013; Richmond et al., 2019] and wakes [Castellani et al., 2013; Sert et al., 2014; Kuo et al., 2016; Behrouzifar and Darbandi, 2019; Antonini et al., 2019] to decrease the complexity of the configuration and computational cost of the simulation. Besides, solver type and turbulence models selection poses a similar dilemma. In addition, the effects of the atmospheric boundary layer [Avila et al., 2013; Antonini et al., 2019], available meteorological wind data [Avila et al., 2013], and topography [Avila et al., 2013; Kuo et al., 2016; Antonini et al., 2020] have been studied in the literature. Besides, several optimization studies [Kuo et al., 2016; Antonini et al., 2020; Saebzadeh et al., 2020] have been conducted by implementing different combinations of the options mentioned above.

Additional to the numerical simulations, there are studies comparing the experimental wake data with the analytical wake models. Polster [2017] examined five analytical models for wake profiles at several downstream locations of the NTNU model turbine and compared their results with the wind tunnel data. It was concluded that some of the models, such as Larsen and Frandsen models, were unable to determine the wake shape, while some, such as Schlichting and Jensen-Gaussian models, were successful in the predictions. Similarly, Kaldelliss et al. [2021] extensively compared nine wind turbine wake models developed between 1983 and 2020. They applied the models to several test cases, including two experimental cases with measurements and a computational one with available LES data. The article concludes that the wake models may be applied to wind farm placement and optimization with a slight deviation from the actual flow behavior.

In this study, an extensive comparison of the wake flow properties of the selected NTNU wind turbine rotor test cases [Bartl et al., 2012; Ceccotti et al., 2016] is made by performing CFD simulations with different turbulence models, transition models, and freestream turbulence intensities. The CFD simulations for two cases are performed, a single-turbine case for validation and a two-turbine case for rotor/rotor interactions and comparisons. Moreover, different analytical models are applied to the selected configurations, and their results are compared with both computational and experimental data.

METHODOLOGY

In this paper, the CFD simulations are performed for the NTNU model turbine [Krogstad and Lund, 2012]. The three-bladed turbine has a rotor diameter of 0.9 m and a hub height of 0.82 m. NREL S826 airfoil is used throughout the rotor blade. The turbine was designed by the BEM method with the Prandtl and Glauert corrections for a reference velocity of 10 m/s, and its optimum operation is obtained at the tip speed ratio of $\lambda = 6$. It was aimed to be used as a test case for computational turbulence models [Pierella et al., 2014].

The CFD simulations are performed by solving the RANS equations by using the Ansys FLUENT commercial CFD software. Similar to the literature, commonly used turbulence models, Spalart Allmaras, standard $k-\epsilon$, standard $k-\omega$, and $k-\omega$ SST models, are used to investigate the effect of turbulence model on the wind turbine wake predictions and compare with the analytical models for different freestream turbulence intensities.

Since the NTNU turbine is a model turbine, it has smaller blades than the commercial wind turbines, so the Reynolds number of the flow on the rotor surface is lower as well, around $Re_{tip} \approx 10^5$. Therefore, the flow around the turbine tends to transition to turbulent flow due to the relatively low Reynolds number. That is why several transition models available in the solver, $k-k_L-\omega$ and Transition SST models, are tested in the simulations.

The CFD simulations for two cases are performed in this study, a single-turbine case for validation and a two-turbine case for rotor/rotor interactions. The configuration of the computational domain used in both simulations, including the rotor, nacelle, and tower for each turbine, is referenced from the experiments conducted by Ceccotti et al. [2016] for the single-turbine case and Bartl et al. [2012] for the two-turbine case. Both experiments were done in the NTNU Wind Tunnel. The test section dimensions are 2.7 x 1.81 x 11.15 [m] for the single-turbine case and 2.7 x 2.0 x 12.0 [m]. The distance between the inlet and the upstream turbine is twice the rotor diameter for the single-turbine case and the rotor diameter for the two-turbine case. In the two turbine case, the downstream turbine is placed three-rotor diameter away from the upstream turbine. Moreover, the hub height of the turbine is increased to 0.95 m for the two-turbine case. The reference wind speed is $U_{ref} = 11.5$ m/s for both cases. The experiments were conducted with two different freestream turbulence intensity values, which are TI=0.23% and TI=10.0%. The freestream flow enters the test section uniformly. In other words, the atmospheric boundary layer is not modeled. The turbine in the single rotor case and the upstream turbine in the two-turbine case operate at $\lambda = 6$ tip speed ratio, while the downstream one in the two-turbine case does at $\lambda = 4$. The wind tunnel walls are included in the simulations with the no-slip boundary condition since the blockage effects in the experiments were indicated as significant for a similar experiment conducted in the same test section [Polster, 2017]. The wind tunnel and the wind turbine are fully resolved and modeled using the exact dimensions of the experimental cases.

Computational Grid

A mesh independence study is done for the single turbine case at a low turbulence intensity level with $k-\omega$ SST turbulence model. Three different grids are created with the cell counts of 1.7 million, 2.9 million, and 5.3 million for coarse, medium, and fine grids, respectively. Wake velocity profile results are obtained at the x/D=5 downstream of the turbine and at the hub height. They are plotted in Fig. 1.

The simulation with the coarse grid fails to predict the flow in the region. Moreover, both the fine and medium grids captured the asymmetric flow trend better than the coarse grid. Also, profiles from the medium and fine grid profiles almost completely match, except the small region of -0.5 $<$ y/D $<$ 0. As a result, in the following analyzes medium grid is used for the single-turbine case to reduce the computational effort. The grid used in the simulations is shown in Figs. 2 and 3 for the single and two-turbine cases, respectively where the cells are colored according to their volumes. There are approximately 9 million cells in the grid for the two-turbine case. A high amount of elements is placed around the wind turbine rotor blades in the rotor grid block and also near the tower to better capture flow details. Also, the wake region, including the, measurement locations are discretized with the fine grid. The Moving Reference Frame (MRF) model represents the rotor grid block with rotating blades in the CFD simulations.

Wake Models

In this study, eight analytical wake models are examined. They are Bastankhah & Porté-Agel [2014], Frandsen [Frandsen et al., 2006], Ishihara [Ishihara et al., 2004], Ishihara & Qian [2018], Jensen [Jensen, 1983; Katic et al., 1986], Jensen Gaussian [Gao et al., 2016], Larsen [Larsen, 1988,

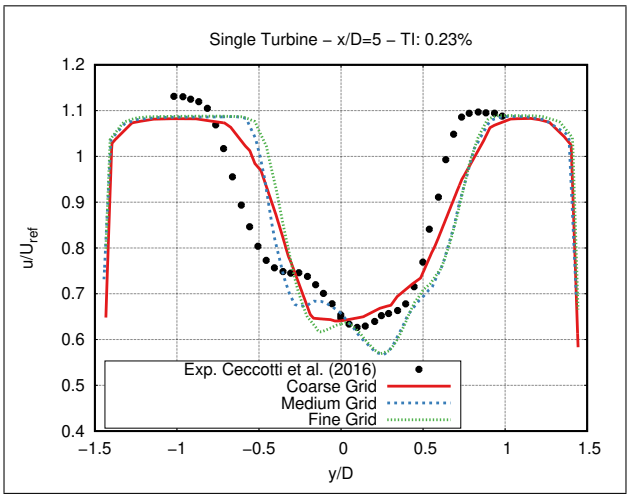

Figure 1: Wake velocity profiles at the hub height for a single turbine configuration for low turbulence intensity (TI=0.23%) and at x/D=5 downstream of the turbine from simulations with different grid density

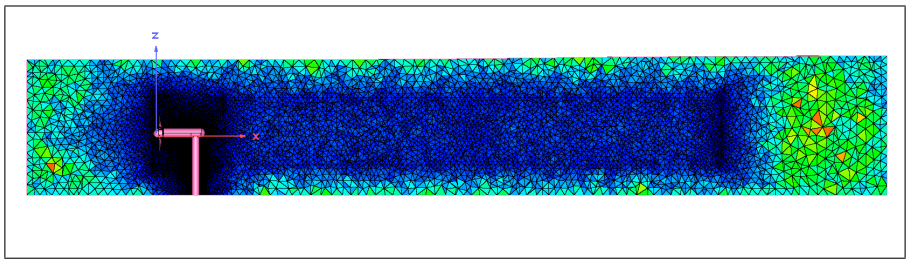

Figure 2: Solution grid for the single-turbine analysis

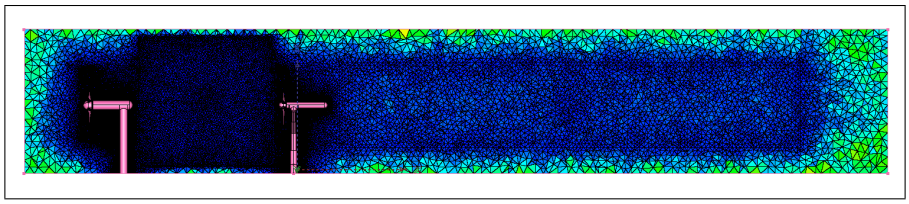

Figure 3: Solution grid for the two-turbine analysis

2009], and Tian [Tian et al., 2015] wake models. The models are selected to investigate a variety of models in terms of both complexity, development year, and accuracy. An overview of the models along with their development year and input parameters is tabulated in Table 1.

Table 1: Overview of the studied wake models

Model	Jensen (Katic)	Larsen	Ishihara	Frandsen	Bastankhah & Porté-Agel	Tian	Jensen Gaussian	Ishihara & Qian
Introduction year	1986	1988	2004	2006	2014	2015	2016	2018
Rotor diameter (D)	+	+	+	+	+	+	+	+
Downstream dist. (x)	+	+	+	+	+	+	+	+
Thrust coeff. (C_T)	+	+	+	+	+	+	+	+
Radial dist. (r)		+	+		+	+	+	+
Wake expansion coeff. (k or k^*)	+			+	+	+	+	
Ambient TI (I_a)		+	+			+	+	+
Wake TI (I_{wake})			+			+	+	
Empirical coeff.		+	+					+

Bastankhah & Porté-Agel Model:

This wake model was developed by applying the conservation of mass and momentum downstream of a wind turbine. The viscous and pressure terms in the conservation of the momentum equation are neglected. Also, the wake velocity distribution is assumed to be in a Gaussian shape. Moreover, a linear expansion is assumed in the wake region. Eq. 1 calculates the wake velocity distribution.

$$\frac{U(x,r)}{U_{ref}} = 1 - \left(1 - \sqrt{1 - \frac{C_T}{8(k^*x/D + \epsilon)^2}}\right) \exp\left(\frac{-r^2}{2D^2(k^*x/D + \epsilon)^2}\right) \tag{1}$$

where y and z are spanwise and vertical coordinates, respectively. Also, D is the rotor diameter, and z_h is the hub height. ϵ is the normalized initial wake half-width. Although the original paper [Bastankhah and Porté-Agel, 2014] gave:

$$\epsilon = 0.25\sqrt{\beta} \tag{2}$$

the authors indicated in the same paper that another constant factor for this parameter fit better to the available LES data and used the modified factor in their later papers [Porté-Agel et al., 2020; Bastankhah et al., 2021].

$$\epsilon = 0.2\sqrt{\beta} \tag{3}$$

where β is the normalized initial wake diameter squared.

$$\beta = \frac{1 + \sqrt{1 - C_T}}{2\sqrt{1 - C_T}} \tag{4}$$

As Table 1 shows, all the models require the thrust coefficient, C_T, known beforehand the computation. For this study, thrust coefficients for all cases are extracted from the experimental data of an experiment in the literature where the same model turbine was placed in a configuration similar to the one in this work [Pierella and Sætran, 2017]. Lastly, k^* is the wake growth rate, and an LES dataset [Niayifar and Porté-Agel, 2016] suggests the following relation.

$$k^* = 0.3837 I_a + 0.003678 \tag{5}$$

Frandsen Model:

The wake model was derived by applying the conservation of momentum equation within a control volume without the unsteady, pressure, gravity, and viscosity terms. Moreover, it is assumed that the pressure at the most downstream location within the control volume would be equal to the freestream level. Moreover, the wake shape is represented by a rectangular distribution. Lastly, the initial wake diameter is assumed to be the same as the rotor diameter.

$$\frac{U(x)}{U_{ref}} = 1 - \left(\frac{1}{2}\left(1 - \sqrt{1 - 2\frac{A_{rotor}}{A_{wake}}C_T}\right)\right) \tag{6}$$

where

$$A_{wake}(x) = \pi\left(\frac{1 + \sqrt{1 - C_T}}{2\sqrt{1 - C_T}} + \frac{\alpha x}{D}\right) D^2 \tag{7}$$

where α is the decay factor and can be taken as $\alpha = 10k$ for small C_T and at long downstream locations. Although, the authors suggested using $k = 0.05$ for the wake expansion coefficient, this value is applicable for large offshore wind farms [Barthelmie et al., 2006]. Since multiple turbulence intensity levels are studied in this work, a definition depending on the ambient turbulence level should be used. Hence, the following relation found in several studies [Kollwitz, 2016; Polster, 2017] is used.

$$k \approx 0.5 I_a \tag{8}$$

Ishihara Model:

The conservation of momentum equation for axial-symmetric flow is considered for the development of this wake model. Moreover, the wake model consists of empirical coefficient values extracted from the wind tunnel experiments with a model wind turbine. In the experiments, the flow consisted of an atmospheric boundary layer generated for both onshore and offshore cases.

$$\frac{U(x,r)}{U_{ref}} = 1 - \left(\frac{\sqrt{C_T}}{32} \left(\frac{1.666}{k_1} \right)^2 \left(\frac{x}{D} \right)^{-p} e^{-r^2/b^2} \right) \tag{9}$$

$$k_1 = 0.27, k_2 = 6.0, k_3 = 0.004 \tag{10}$$

$$b(x) = \frac{k_1 C_T^{0.25}}{0.833} D^{1-p/2} x^{p/2} \tag{11}$$

where p shows the rate of wake recovery, which takes both the ambient turbulence and the turbulence generated by the wind turbine into account.

$$p = k_2 (I_a + I_{wake}) \tag{12}$$

$$I_{wake} = k_3 \frac{C_T}{max(I_a, 0.03)} \left(1 - \exp\left(-4 \left(\frac{x}{10D} \right)^2 \right) \right) \tag{13}$$

Ishihara & Qian Model:

The Ishihara & Qian Model is derived similarly to the Ishihara Model and the Bastankhah & Porté-Agel Model. While the wake velocity profile has a Gaussian shape, the wake expanses linearly. The streamwise function, which represents the maximum normalized velocity deficit at a given downstream location, is modified compared to Bastankhah & Porté-Agel Model. In this model, a first-order approximation from the Taylor Series expansion of the term is taken to avoid divergence near the rotor.

$$\frac{U(x,r)}{U_{ref}} = 1 - \left(\frac{1}{\left(a + bx/D + c(1 + x/D)^{-2} \right)^2} \exp\left(-\frac{r^2}{2\sigma^2} \right) \right) \tag{14}$$

$$\sigma = k^* x + \epsilon D \tag{15}$$

The expressions given below are derived by fitting the experimental and LES datasets.

$$k^* = 0.11 C_T^{1.07} I_a^{0.20} \quad \epsilon = 0.23 C_T^{-0.25} I_a^{0.17}$$

$$a = 0.93 C_T^{-0.75} I_a^{0.17} \quad b = 0.42 C_T^{0.6} I_a^{0.2} \quad c = 0.15 C_T^{-0.25} I_a^{-0.7}$$

$$d = 2.3 C_T^{-1.2} \qquad e = I_a^{0.1} \qquad f = 0.7 C_T^{-3.2} I_a^{-0.45}$$

Jensen Model:

In the original Jensen Model [Jensen, 1983], the wake velocity distribution is assumed to be one-dimensional and the wake expands linearly with a constant speed recovery. Moreover, the effect of tip vortices are neglected. However, the attributes of the rotor is not included in the original model. Later, it was modified to do so [Katic et al., 1986].

$$\frac{U(x)}{U_{ref}} = 1 - \frac{1 - \sqrt{1 - C_T}}{(1 + 2kx/D)^2} \tag{16}$$

Jensen Gaussian Model:

This model converts the constant velocity profile in the Jensen Model to a profile with Gaussian distribution. The wake radius is taken equal to the one in the Jensen Model with the difference that velocity at the edge of the wake is equal to the freestream velocity. Moreover, the mass flow from this model is the same as in the Jensen model. In addition, the model implements an empirical wake turbulence term depending on the downstream location for the wake decay constant.

$$\frac{U^*(x)}{U_{ref}} = 1 - \frac{2a}{\left(1 + \frac{k_{wake}x}{r_1}\right)^2} \tag{17}$$

$$\frac{U(x,r)}{U_{ref}} = 1 - \left(1 - \frac{U^*(x)}{U_{ref}}\right) \frac{5.16}{\sqrt{2\pi}} \exp\left(\frac{-r^2}{2(r_x/2.58)^2}\right) \tag{18}$$

where U^* is the velocity distribution from the Jensen model, expect the wake decay constant k_{wake}:

$$k_{wake} = k\frac{I_{wake}}{I_a} \tag{19}$$

$$I_{wake} = \left(K_n \frac{C_T}{\sqrt{x/D}} + \sqrt{I_a}\right)^2 \tag{20}$$

The relation for wake turbulence, I_{wake} is empirical and developed to balance the effect of the ambient turbulence and the turbulence within the wake. K_n constant is assumed to be 0.4 in the model. Moreover, a is the induction factor:

$$a = \frac{1 - \sqrt{1 - C_T}}{2} \tag{21}$$

Also, r_1 is the initial wake radius:

$$r_1 = \frac{D}{2}\sqrt{\frac{1-a}{1-2a}} \tag{22}$$

Lastly, r_x is the wake radius at a given downstream location.

$$r_x(x) = \frac{D}{2} + k_{wake}x \tag{23}$$

Larsen Model:

The Larsen Model is derived from Prandtl's boundary layer equations. While the pressure term is neglected, the Reynold stress term is approximated by applying Prandtl's mixing length theory. Then, the simplified boundary layer equations are substituted into the conservation of momentum equation applied to an infinitely large control volume containing the rotor. Lastly, the obtained expression is solved with the continuity equation in the RANS equations. The modified version [Larsen, 2009] defines the boundary conditions at the rotor plane and the plane placed at 9.6D downstream of the rotor.

$$\frac{U(x,r)}{U_{ref}} = 1 - \frac{1}{9}\left(C_T A_0 (x + x_0)^{-2}\right)^{1/3} \left(r^{3/2}\left(3c_1^2 C_T A_0 (x + x_0)\right)^{-1/2} - \left(\frac{35}{2\pi}\right)^{3/10}\left(3c_1^2\right)^{-1/5}\right)^2 \tag{24}$$

where

$$x_0 = \frac{9.6D}{(2R_{9.6}/kD)^3 - 1} \tag{25}$$

$$c_1 = \left(\frac{kD}{2}\right)^{5/2}\left(\frac{105}{2\pi}\right)^{-1/2}\left(C_T A_{rotor} x_0\right)^{-5/6} \tag{26}$$

$$k = \sqrt{\frac{1}{2\sqrt{1-C_T}} + \frac{1}{2}} \tag{27}$$

Furthermore, $R_{9.6}$ is the wake radius at 9.6 rotor diameter downstream. It is approximated with empirically determined coefficients.

$$R_{9.6} = a_1 \exp\left(a_2 C_T^2 + a_3 C_T + a_4\right)(b_1 I_a + 1)D \tag{28}$$

$$a_1 = 0.435449861 \quad a_2 = 0.797853685 \quad a_3 = -0.124807893$$

$$a_4 = 0.136821858 \quad b_1 = 15.6298$$

Tian Model:

This wake model is based on the original Jensen Model. It modifies the model similar to how Jensen Gaussian Model does. Differently, the Tian Model implements a 2D cosine velocity distribution instead of the Gaussian distribution. Moreover, this model proposes another wake turbulence intensity that depends on both the ambient turbulence and the turbulence created by the turbine.

$$\frac{U^*(x)}{U_{ref}} = 1 - \frac{2a}{\left(1 + \frac{k_{wake}x}{r_1}\right)^2} \tag{29}$$

$$\frac{U(x,r)}{U_{ref}} = \left(1 - \frac{U^*(x)}{U_{ref}}\right)\cos\left(\frac{\pi r}{r_x} + \pi\right) + \frac{U^*(x)}{U_{ref}} \tag{30}$$

The parameter definitions are rather similar to those in the Jensen Gaussian Model. The only difference is in the empirical wake turbulence intensity relation:

$$I_{wake} = K_n \frac{C_T}{(x/D)} + I_a \tag{31}$$

Blockage Correction Factor in Wake Model Results

The analytical wake models have usually been developed for wind farm applications. In other words, the solution domain should be unbounded, except the ground. Thus, the flow velocity tends to reach the freestream velocity outside the wake. However, since there is limited area inside the wind tunnel due to the test section walls, the flow attributes inside that limited area in the wind tunnel could be changed, whereas this is not the case for the wind farm environment. This disturbance is called blockage interference [Ewald, 1998]. Hence, the flow velocity could be greater than the reference velocity near the tunnel walls.

The experiments conducted in the NTNU Wind Tunnel with the NTNU Model Wind Turbine, and the computational studies replicating the same configuration reveal that the blockage factor is too significant to be neglected [Krogstad and Eriksen, 2013; Schümann et al., 2013; Pierella et al., 2014; Martínez-Tossas et al., 2015; Bartl and Sætran, 2016; Pierella and Sætran, 2017; Polster, 2017; Mühle et al., 2018]. In this work, the blockage correction factor for each wake model is calculated by applying the continuity equation. Assuming the flow is incompressible, the average velocity at each cross-section should be equal to the freestream velocity to ensure the conservation of mass. Hence, the velocity at all the discrete points at each downstream location is multiplied by the following factor, $\gamma(x)$:

$$\gamma(x) = \frac{U_{ref}}{\frac{1}{A(x)}\iint_{A(x)} U dA} = \frac{U_{ref}}{U_{mean}(x)} \tag{32}$$

where $A(x)$ is the cross-sectional area of the test section, which is equal to 4.887 m^2 and 5.4 m^2 for the single and two-turbine cases, respectively. Fig. 4 compares the blockage correction factors for each wake model results for the single-turbine case with high turbulence intensity. Besides, Polster [2017] implements a method developed by Ryi et al. [2015] for the blockage correction of the experiment having the same configuration as the single-turbine configuration in this work. He found the correction factor as 1.0525, which is plotted as a black horizontal line in Fig. 4. Although there are significant differences near the turbine, almost all the models, except the Jensen Model, agree with the factor found by Polster [2017] away from the turbine. In addition, the correction factor decreases at more downstream locations for most models, which shows the diffusion of the wake.

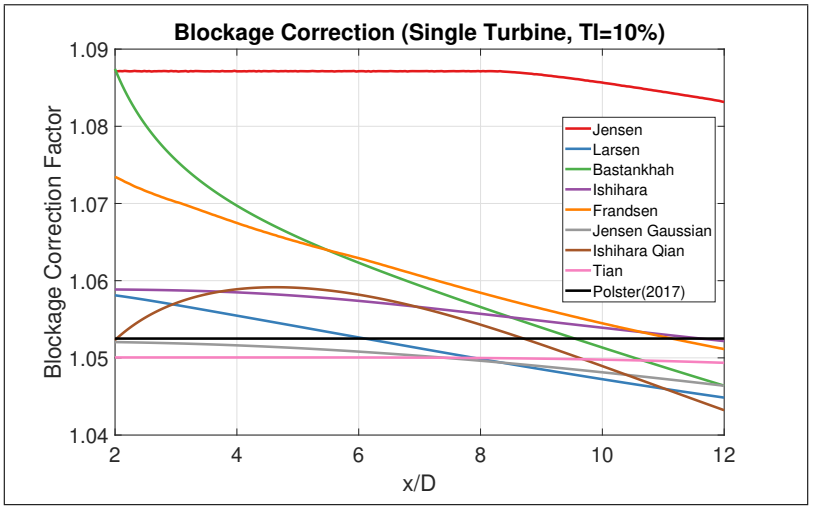

Figure 4: Blockage correction factor for each wake model computed by the continuity equation with the incompressibility assumption for the single-turbine case at TI=10% along with the factor computed by Polster [2017].

Wake Superposition in the Wake Models

The wake velocity distribution for the two-turbine case is determined by calculating the individual turbine wakes separately, then for each calculated point, the velocity is calculated by combining the wakes passing that point with a superposition method. Some of the commonly utilized superposition methods are listed below.

1) Linear sum (Global) [Lissaman, 1979] : $\frac{U(x,y,z)}{U_{ref}} = 1 - \sum_{i=1}^{n} \left(1 - \frac{U_i(x,y,z)}{U_{ref}}\right)$

2) Linear sum (Local) [Niayifar and Porté-Agel, 2016] : $\frac{U(x,y,z)}{U_{ref}} = 1 - \sum_{i=1}^{n} \left(\frac{U_{iw}}{U_{ref}} - \frac{U_i(x,y,z)}{U_{ref}}\right)$

3) Root sum square (Global) [Katic et al., 1986] : $\frac{U(x,y,z)}{U_{ref}} = 1 - \sqrt{\sum_{i=1}^{n} \left(1 - \frac{U_i(x,y,z)}{U_{ref}}\right)^2}$

4) Root sum square (Local) [Voutsinas et al., 1990] : $\frac{U(x,y,z)}{U_{ref}} = 1 - \sqrt{\sum_{i=1}^{n} \left(\frac{U_{iw}}{U_{ref}} - \frac{U_i(x,y,z)}{U_{ref}}\right)^2}$

where U_{iw} is the local average velocity within the rotor swept area incoming to the turbine i. For the upstream turbine, it is the reference velocity, while the downstream turbine faces a lower velocity because it encounters the wake of the upstream turbine.

Not only the incoming velocity but also the turbulence level the downstream turbine faces are altered due to the upstream turbine. The Ishihara, Jensen Gaussian, and Tian Models calculate the wake turbulence level within the wake. For the downstream turbine, the ambient turbulence level is replaced with the wake turbulence level at the location where the downstream turbine is located from the upstream turbine calculations. However, the ambient turbulence intensity level is implemented

for both turbines in the remaining models since they do not contain any relation regarding the wake turbulence level.

RESULTS AND DISCUSSIONS

The wake shapes obtained from the steady-state simulations using various turbulence and transition models are compared at several downstream locations. Additionally, the wake shapes obtained from the analytical models are plotted with the simulation results, and their validity is discussed. Moreover, the 2D velocity contours from both simulations and wake models are given and discussed.

Single-Turbine Case

The single-turbine case is analyzed with multiple turbulence models: Spalart Allmaras, standard $k-\epsilon$, standard $k-\omega$, and $k-\omega$ SST models. The obtained results are compared with the available experimental results [Ceccotti et al., 2016] at two different turbulence intensity levels, 0.23% and 10%. Wake velocity profiles at x/D=3, x/D=5, and x/D=9 downstream of the turbine and at the hub height are presented in Figs. 5 and 6 for the low and high turbulence levels, respectively.

As seen from the Fig. 5, all turbulence models are able to capture the two peak regions of the experimental results at location x/D=3. In addition to that, asymmetric behavior present in the experimental result is obtained by the turbulence models. On the other hand, at location x/D=5 turbulence models overestimated the peak velocity deficit and created multiple velocity deficit peak points which are not observed in the experiments, but $k-\omega$ SST and Spalart-Allmaras turbulence models predicted flow closer to the experiments compared to the standard $k-\epsilon$ and standard $k-\omega$ models. Overestimation of the velocity deficit is also observed at the x/D=9 location, showing that the diffusion rate of the wake in the experiment could not be captured well by any of the models. However, the velocity profile is getting to a Gaussian shape at more downstream locations in both experimental and computational data. Moreover, the simulations underestimate the wind tunnel blockage factor since the velocity near the test section walls from the CFD simulations is lower than the one in the experimental data. The results show that the $k-\omega$ SST turbulence model could be the most right choice for such a configuration as the Spalart-Allmaras model could be considered as another accurate model at such a low turbulence level.

For the high turbulence intensity flow, obtained results are compared in Fig. 6. There are slight changes in the velocity profiles in terms of magnitude in the experimental data, but the shape of the velocity distribution is closer to the symmetrical Gaussian shape due to the higher diffusion rate because of the high ambient turbulence intensity. The simulation results show the same difference, but at a lower rate, except the Spalart-Allmaras model, which is the only one giving the Gaussian

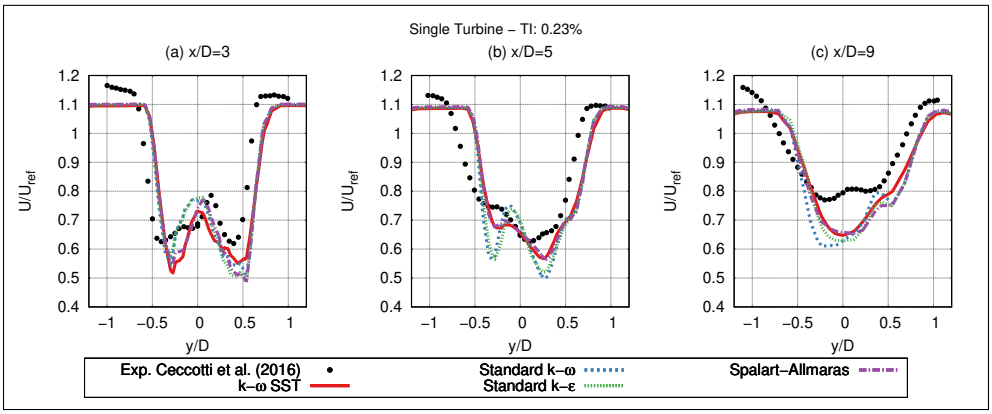

Figure 5: Wake velocity profiles at the hub height for the single-turbine configuration for low turbulence intensity (TI=0.23%) and at x/D=3 *(a)*, x/D=5 *(b)*, and x/D=9 *(c)* downstream of the turbine from $k-\omega$ *SST*, Standard $k-\epsilon$, Standard $k-\omega$, and Spalart-Allmaras turbulence models

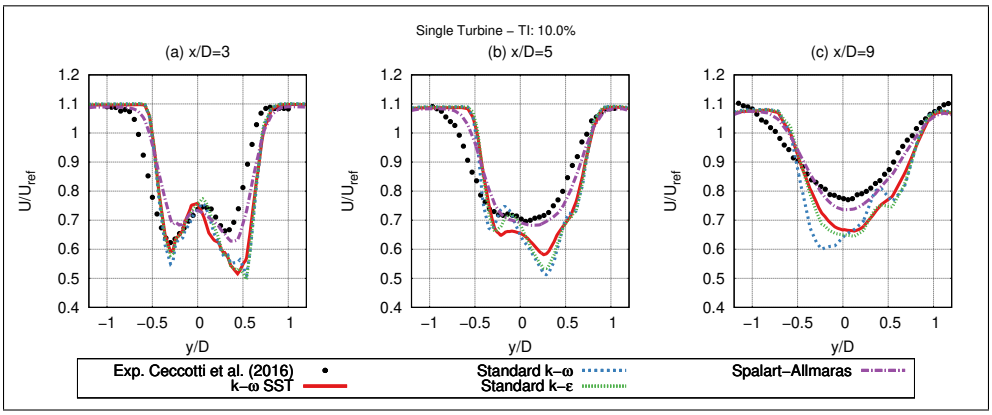

Figure 6: Wake velocity profiles at the hub height for the single-turbine configuration for high turbulence intensity (TI=10.0%) and at x/D=3 *(a)*, x/D=5 *(b)*, and x/D=9 *(c)* downstream of the turbine from $k-\omega$ *SST*, Standard $k-\epsilon$, Standard $k-\omega$, and Spalart-Allmaras turbulence models

shape away from the turbine. In addition, the blockage effect is captured validly by all the models. Although the $k-\omega$ SST turbulence model can still be considered as a probable candidate, the Spalart-Allmaras model gives the velocity profile closest to the experiments.

NTNU turbine is a scaled wind turbine; thus, it operates at low Reynolds numbers. Therefore, laminar to turbulent transition can play an essential role in the results. To examine the transition effects, $k-\omega$ SST and the results from the experiments [Ceccotti et al., 2016] are compared with the $k-k_L-\omega$, and Transition SST transition turbulence model findings for the low turbulence intensity flow in Fig. 7. At all downstream locations, $k-k_L-\omega$ turbulence model captured a similar velocity deficit level with the experimental results. However, because of the unsteadiness of the flow physics, artificial peak locations are created with this turbulence model. In other words, this model could not capture the Gaussian flow shape away from the turbine. Contrarily, the Transition SST turbulence model agrees with the $k-\omega$ SST turbulence model in all locations except x/D=5 where the $k-\omega$ SST determines the velocity profile closer to the experiments.

The velocity profiles from the wake models are compared with the experimental data and the profile from the $k-\omega-SST$ model in Fig. 8 for low turbulence intensity and in Fig. 9 for high turbulence intensity. The models fail to predict a valid profile at a low turbulence level in Fig. 8 because they cannot predict the diffusion rate correctly. Only the Ishihara model can determine the velocity

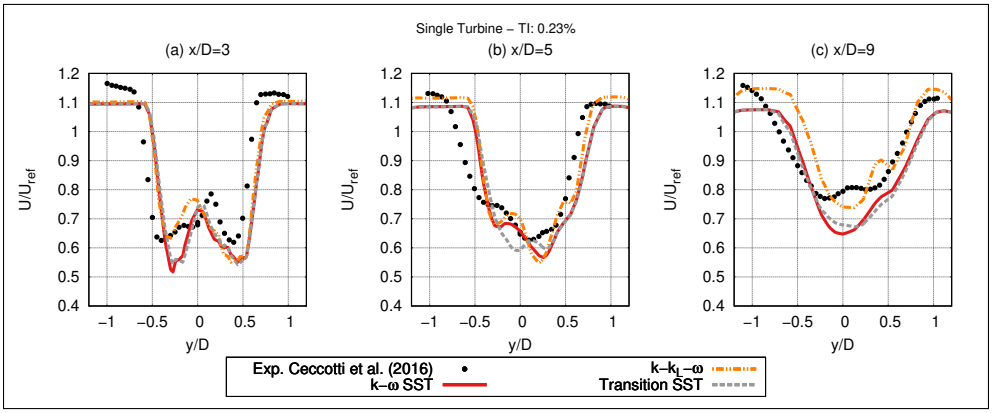

Figure 7: Wake velocity profiles at the hub height for the single-turbine configuration for low turbulence intensity (TI=0.23%) and at x/D=3 *(a)*, x/D=5 *(b)*, and x/D=9 *(c)* downstream of the turbine from $k-\omega$ *SST*, $k-k_L-\omega$, and Transition SST models

profile and the diffusion rate in an acceptable way away from the turbine. The reason could be that this model was developed empirically from the experimental data at a low (TI=3%) and a high (TI=13%) turbulence intensity level [Ishihara et al., 2004]. The remaining models were developed either empirically with wind farm data or analytically with empirical coefficients from wind farm applications. The turbulence intensity levels would not be as low as 0.23% in real-life wind farm applications. In other words, such a low turbulence level in a wind tunnel cannot be observed in a wind farm environment. Thus, almost all of the examined models cannot predict the flow around a wind turbine operating inside a wind tunnel with a low ambient turbulence level.

At the high turbulence intensity level, the wake models can predict both the wake diffusion rate and the velocity deficit in magnitude close to the experimental and CFD results. Since the models do not take the effect of non-rotor components (nacelle, tower), any model cannot predict the unsymmetrical velocity profile, as the CFD simulation can at both turbulence intensity levels near the turbine (x/D=3). Away from the turbine (x/D=5 and x/D=9), the Tian, Jensen Gaussian, and Ishihara wake models are the most valid models compared to the experimental profiles. Moreover, the Bastankhah & Porté-Agel and Ishihara & Qian models gave an acceptable prediction near the turbine, but they highly underestimated the velocity deficit at more downstream location due to the too much wake diffusion rate. In addition, the Jensen Model could be taken as a valid model in terms of the average velocity deficit, but its theory is too simple to determine the velocity profile shape validly. Nonetheless, the Larsen and Frandsen model highly underpredicted both the velocity deficit and wake diffusion rate.

The velocity deficit in the vertical direction on the plane passing through the center of the turbine are plotted at several downstream locations for the $k-\omega-SST$ simulation and the wake model results in Fig. 10 for low turbulence intensity and in Fig. 11 for high turbulence intensity. In these plots, z=0 corresponds to the center of the rotor. In the computational result, the tower shadow is clear from the higher velocity deficit near the ground at x/D=1. However, this effect decays and eventually disappears at more downstream locations for both turbulence conditions.

Although some models predict the velocity deficit in the vertical direction well away from the turbine at the high turbulence level, they fail at the low turbulence intensity level as in the horizontal direction, except the Ishihara model. At the high ambient turbulence level, the Ishihara model cannot give a logical velocity deficit profile near the turbine (x/D=1), but it predicts the maximum velocity deficit well at x/D=2 and x/D=3 along with the Bastankhah, Ishihara Qian, Jensen Gaussian, and Tian models. Nonetheless, the Bastankhah and Ishihara models overpredict the wake diffusion rate since it gives a very low velocity deficit away from the turbine compared to the CFD simulation. In addition, both the Frandsen and Larsen models fail to give a valid velocity profile as in the horizontal case.

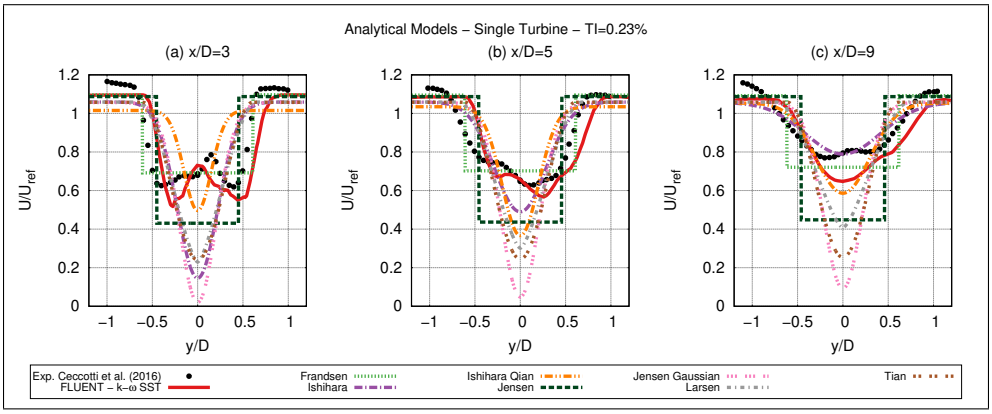

Figure 8: Wake velocity profiles at the hub height for the single-turbine configuration for low turbulence intensity (TI=0.23%) and at x/D=3 *(a)*, x/D=5 *(b)*, and x/D=9 *(c)* downstream of the turbine from CFD simulations with $k-\omega$ SST turbulence model, and analytical wake models

Besides, the Jensen model overly underpredicts the average velocity deficit in the vertical direction contrary to the horizontal case. Nevertheless, the Tian model gives the closest velocity profile away from the turbine (x/D=7 and x/D=9), as the Jensen Gaussian model also computes the profile fairly close to the $k-\omega-SST$ simulation.

Since the tower is not modeled in the wake models, the velocity deficit curves from the analytical models have a Gaussian shape. Hence, it is not possible to model the unsymmetrical wake near the turbine without the sophisticated CFD tools. However, the analytical wake models are able to give valid results away from the turbine and validly determines the average and maximum velocity deficits near the turbine at high turbulence intensity levels.

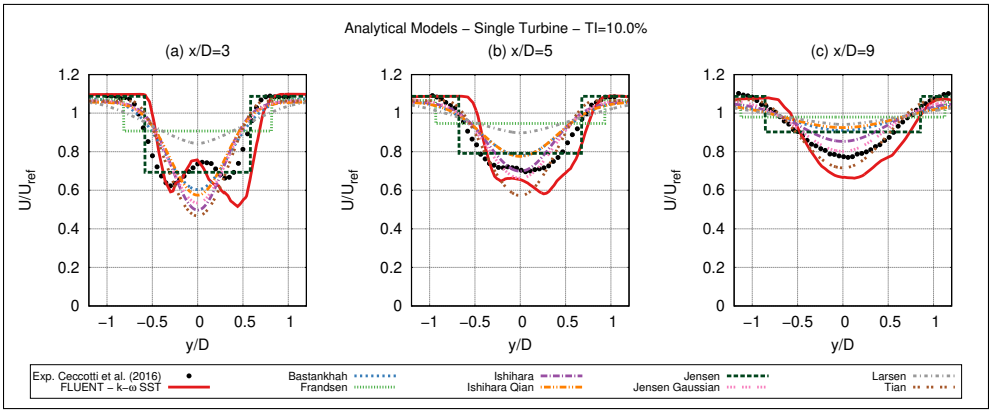

Figure 9: Wake velocity profiles for the single-turbine configuration for high turbulence intensity (TI=10.0%) and at x/D=3 *(a)*, x/D=5 *(b)*, and x/D=9 *(c)* downstream of the turbine from CFD simulations with $k-\omega$ SST turbulence model, and analytical wake models

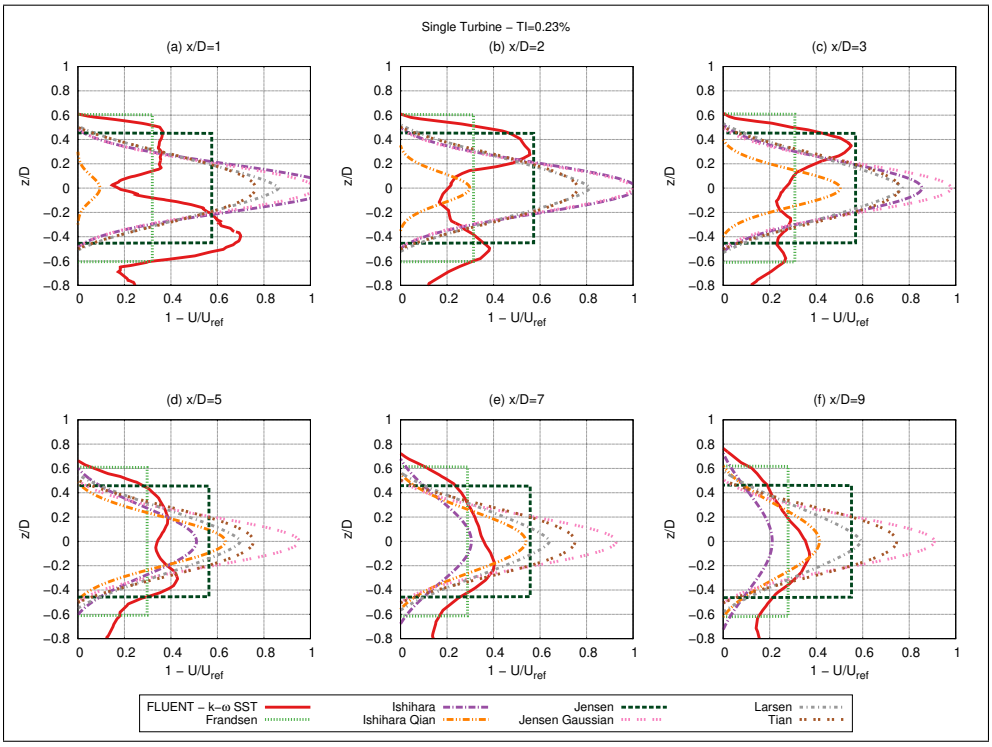

Figure 10: Wake velocity deficit in vertical direction for the single-turbine configuration for low turbulence intensity (TI=0.23%) and at x/D=1 *(a)*, x/D=2 *(b)*, x/D=3 *(c)*, x/D=5 *(d)*, x/D=7 *(e)*, and x/D=9 *(f)* downstream of the turbine from the CFD simulation with $k-\omega$ SST turbulence model, and analytical wake model analysis

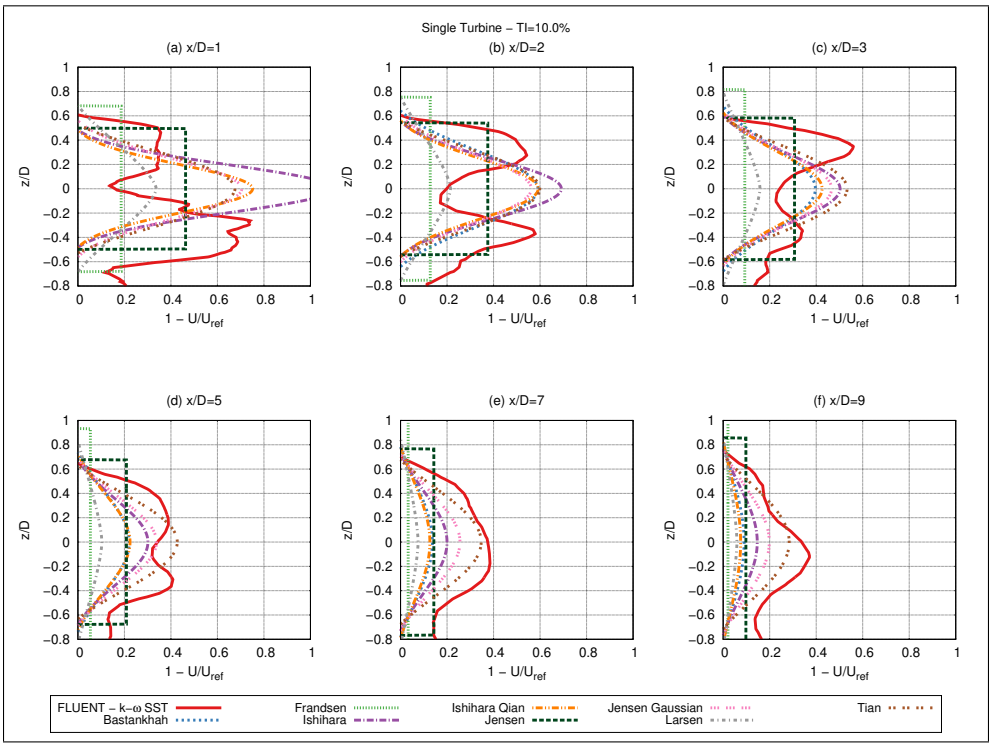

Figure 11: Wake velocity deficit in vertical direction for the single-turbine configuration for high turbulence intensity (TI=10.0%) and at x/D=1 *(a)*, x/D=2 *(b)*, x/D=3 *(c)*, x/D=5 *(d)*, x/D=7 *(e)*, and x/D=9 *(f)* downstream of the turbine from the CFD simulation with $k-\omega$ *SST* turbulence model, and analytical wake model analysis

The velocity distribution on the plane passing through the hub center (y=0) is shown in Figs. 12 and 13 from the CFD simulations and analytical wake models, respectively. The vertical wind tunnel blockage is clear from the velocity distribution above the wake being greater than the reference velocity in all the CFD contours. The blockage shrinks as the flow moves downstream due to the wake expansion and diffusion. The same case is forced in the analytical wake models by applying the blockage factor correction from the conservation of mass.

The tower shadow causes asymmetry in the vertical velocity distribution. However, its effect depends on the turbulence or transition model. While the results from the $k-\omega$ SST and Transition SST have greater and longer velocity deficit in the tower wake, Spalart-Allmaras simulations detect a weaker effect. In addition, the turbulence intensity has an only minor impact on the CFD simulation results. The only exception is the Spalart-Allmaras simulation where the wake diffusion is increased with the greater TI level.

The velocity contours from the analytical wake models start from the turbine location (x=0). Contrary to the CFD results, the velocity distribution is highly affected by the ambient turbulence. The Frandsen, Jensen, Jensen Gaussian, Larsen, and Tian models give nearly negligible wake expansion and diffusion at the low TI level. While Ishihara & Qian model gives an illogical wake shape, the Bastankhah model could not generate a velocity distribution in real numbers throughout the solution domain. Similarly, it could solve the velocity distribution starting from x/D≈1.4 for the high TI level. The only valid velocity contour at the low ambient turbulence is the one from the Ishihara model, as stated for the results given earlier.

As the one-dimensional velocity distributions presented earlier show, the Ishihara, Jensen Gaussian, and Tian models give reasonable velocity contours on the center plane in the high TI results. While the Tian model predicts the wake diffusion to start at a more downstream location, the Ishihara model computes negative velocity near the turbine (x/D<1). In addition, the Bastankhah model

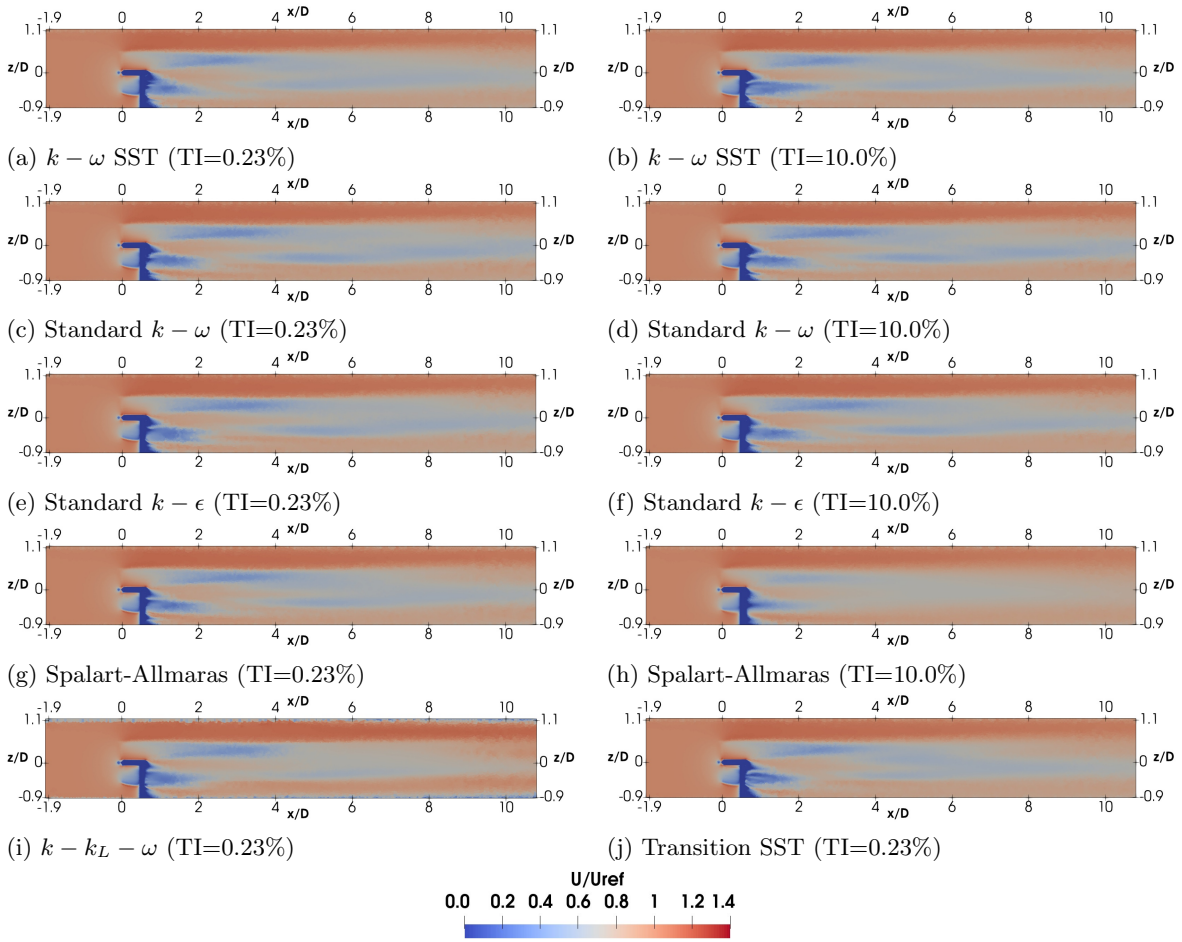

(a) $k-\omega$ SST (TI=0.23%) (b) $k-\omega$ SST (TI=10.0%)

(c) Standard $k-\omega$ (TI=0.23%) (d) Standard $k-\omega$ (TI=10.0%)

(e) Standard $k-\epsilon$ (TI=0.23%) (f) Standard $k-\epsilon$ (TI=10.0%)

(g) Spalart-Allmaras (TI=0.23%) (h) Spalart-Allmaras (TI=10.0%)

(i) $k-k_L-\omega$ (TI=0.23%) (j) Transition SST (TI=0.23%)

Figure 12: 2D normalized velocity contours on the plane passing hub center (y=0) from the CFD simulations for the single-turbine case

gives a logical result, but with a quite high wake diffusion. Moreover, the Larsen model highly overpredicts the wake diffusion since the velocity deficit becomes nearly zero before the flow reaches to the end of the solution domain. In addition, the Ishihara Qian model gives the maximum velocity deficit not at the rotor location which is wrong according to the CFD results in Fig. 12. Lastly, the Frandsen model predicts the wake diameter too large.

Two-Turbine Case

The empirical wake superposition methods are compared with each other and the experimental data through the wake velocity profiles at several downstream locations behind the second turbine in Fig. 14. The velocity profiles are generated by the Tian wake model. While the global methods (Lissaman and Katic et al.) cause a discontinuity in the velocity distribution at the edge of the wake caused by the downstream turbine, which is not present in the experimental results, the local methods (Niayifar & Porté-Agel and Voutsinas et al.) ensure the continuity in the profile. Moreover, the global linear sum method (Lissaman) extremely overestimates the velocity deficit. Although the global root sum square method (Katic et al.) predicts the maximum velocity deficit quite well, it fails to match the experimental average velocity deficit due to the overestimation between the rotor swept area and the wake from the downstream turbine, and the excessive blockage correction factor. The local linear sum (Niayifar & Porté-Agel) and local root sum square (Voutsinas et al.) methods predict the velocity profile shape reasonably accurately, but both underestimate the velocity deficit. Nevertheless, this could be because a blockage correction was applied to the experimental data since

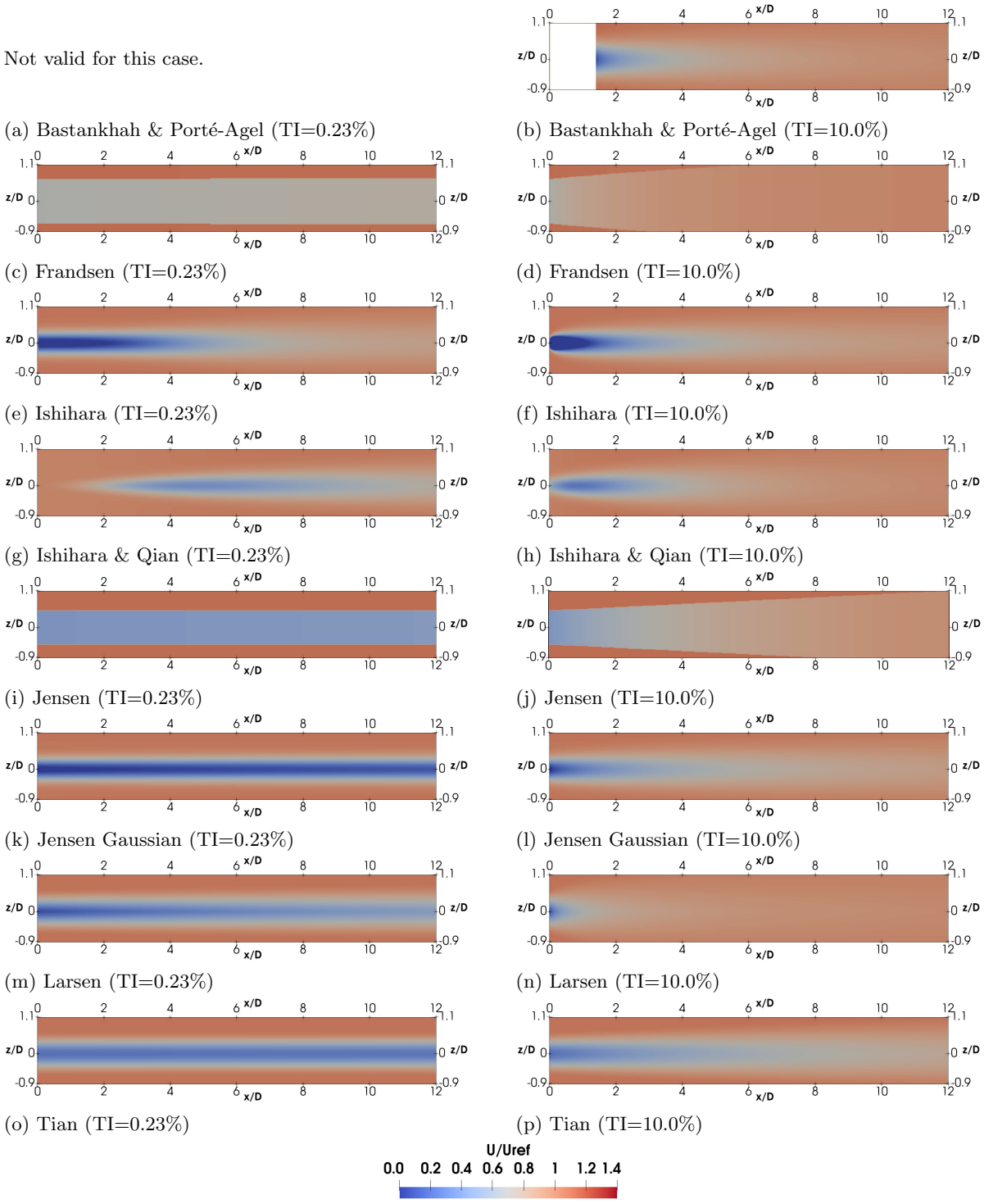

Figure 13: 2D normalized velocity contours on the plane passing hub center (y=0) from the wake models for the single-turbine case

the velocity distribution goes to the reference velocity near the tunnel walls which should have been greater. However, this was not explained in the original paper [Bartl et al., 2012].

The wake velocity profile at several downstream locations for the two-turbine case from the experimental data, the CFD simulation with the $k-\omega$ SST turbulence model, and the analytical wake

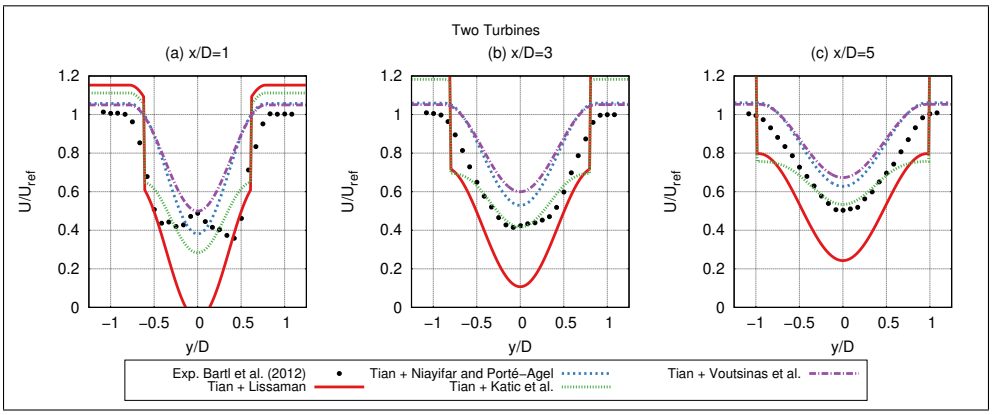

Figure 14: Wake velocity profiles for the two-turbine configuration for high turbulence intensity (TI=10.0%) and at x/D=1 *(a)*, x/D=3 *(b)*, and x/D=5 *(c)* downstream of the second turbine from the Tian wake model combined with the Lissaman, Niayifar & Porté-Agel, Katic et al., and Voutsinas et al. wake superposition methods compared with the available experimental data

models with the Niayifar & Porté-Agel superposition method is plotted in Fig. 15. It is shown that the wake models cannot capture the flow near the configuration in shape. As in the single turbine case, high-fidelity CFD simulations are needed to capture the flow near the turbine since the analytical wake methods do not model the non-rotor components. The CFD simulation considerably captures the unsymmetrical velocity profile. However, the simulation gives local peaks near the turbine (x/D=1), which are not present in the experimental data. Away from the turbine, the CFD simulation determines the wake diffusion remarkably well, but it calculates the maximum velocity deficit slightly higher than the experiments. Moreover, it underestimates the velocity deficit within most of the plot, resulting in a greater average speed. This finding suggests that higher-fidelity simulations like DES or LES could be required to replicate the flow within the large wind farms.

All the wake models underestimate the average velocity deficit away from the turbine. Especially, the Frandsen, Larsen, and Jensen models cannot accurately give the velocity deficit at all the downstream locations. Tian, Jensen Gaussian, and Ishihara Qian models determine the velocity profile shape quite close to the experimental ones, but they overestimate the velocity distribution. Nevertheless, the experimental profile could be shifted upward if the possible blockage correction was not applied, making the Tian model result acceptable compared to the experimental data. Moreover, the Ishihara model predicts the maximum velocity deficit quite close to the experimental one, although it cannot accurately give the proper Gaussian shape.

The velocity deficit curves in the vertical direction are plotted for the CFD simulation and the analytical wake models at several downstream locations in Fig. 16. The CFD simulations show that the tower shadow has a significant effect on the velocity distribution. Note that the tower shadow is more significant in Fig. 11 for the single turbine case. In this case, the velocity deficit from the rotor and tower is very close because the tower wake diffuses more rapidly, as can be seen in the (c) x/D=3 plot in Fig. 11 where the second turbine is located in the two-turbine case. This suggests that rotor/rotor and tower interactions within a wind farm are quite significant, and the modeling of such components is crucial. Nevertheless, the vertical velocity distribution becomes similar at x/D=7 and x/D=9 downstream of the turbine for both single and two-turbine cases which implies that the effect of the turbine components may diminish sufficiently away from the turbine. Thus, the computational simulation on a wind farm could be adjusted according to the placement of the turbines. While a dense array may require more detailed modeling, a simulation with less detailed component modeling could be sufficient for a sparse wind farm.

Starting from x/D=5 downstream location, the analytical wake models give wake profile shapes similar to the ones from the CFD simulations since the velocity distribution becomes close to the Gaussian shape. However, the analytical wake model profiles center around the hub center, while

the CFD simulation profile does around a location slightly closer to the ground. This difference is also present in the single turbine results shown in Fig. 11. Thus, the blockage from the wind tunnel roof may affect the vertical velocity distribution the turbines face. However, the wake models lack of such an effect. Overall, the Ishihara model gives the closest velocity profile to the computational simulation results, as the Tian model computations could be mentioned as an acceptable result.

Two-turbine case results on the plane passing through the center of the wind turbines (y=0) from the CFD simulation and analytical wake models are shown in Fig. 17. Analytical wake model results

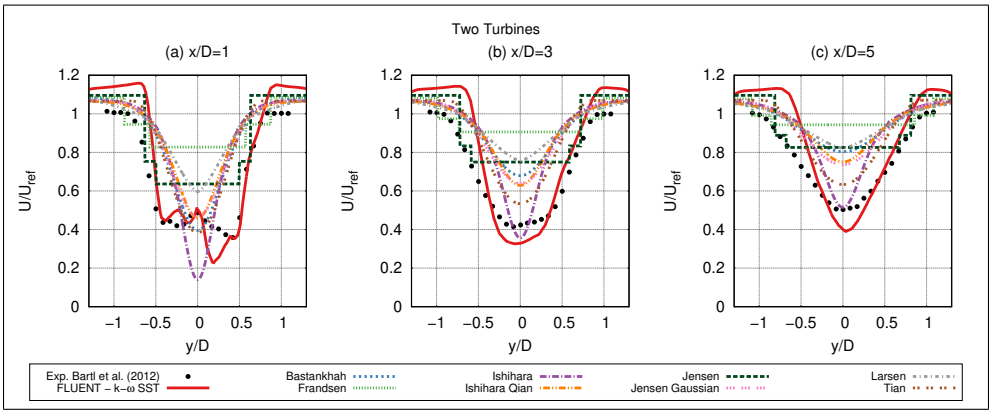

Figure 15: Wake velocity profiles for the two turbine configuration for high turbulence intensity (TI=10.0%) and at x/D=1 *(a)*, x/D=3 *(b)*, and x/D=5 *(c)* downstream of the second turbine from the available experimental data, the CFD simulation with the $k-\omega$ *SST* turbulence model and the analytical wake models with the Niayifar & Porté-Agel superposition model

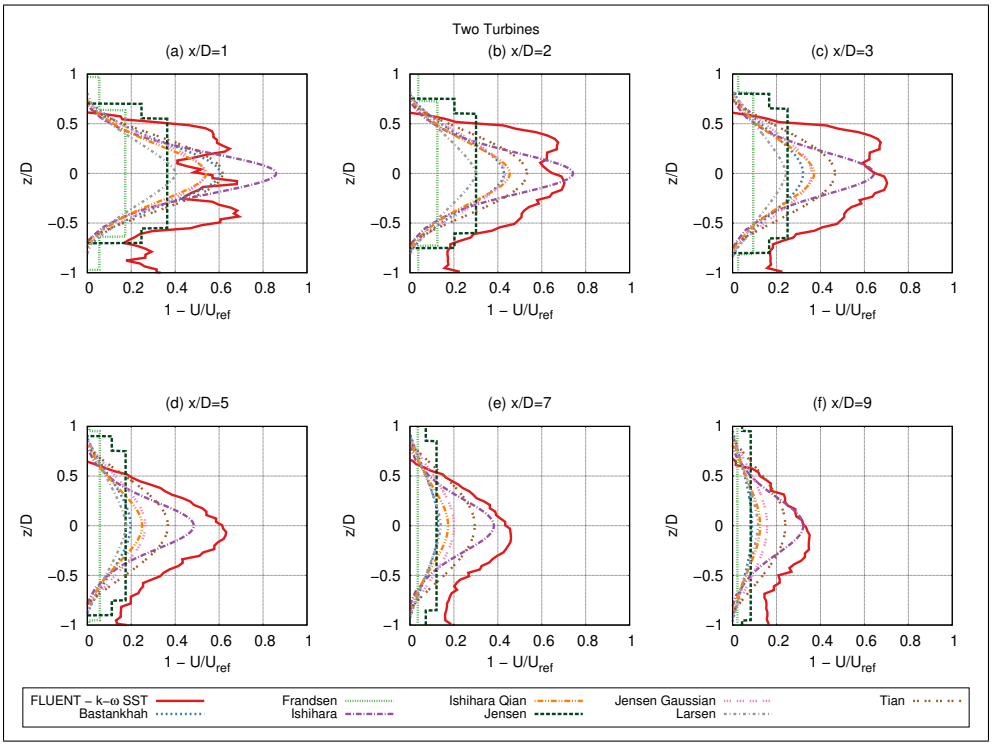

Figure 16: Wake velocity deficit in vertical direction for the two-turbine turbine configuration for high turbulence intensity (TI=10.0%) and at x/D=1 *(a)*, x/D=2 *(b)*, x/D=3 *(c)*, x/D=5 *(d)*, x/D=7 *(e)*, and x/D=9 *(f)* downstream of the second turbine from the CFD simulation with $k-\omega$ *SST* turbulence model, and analytical wake models with the Niayifar & Porté-Agel superposition model

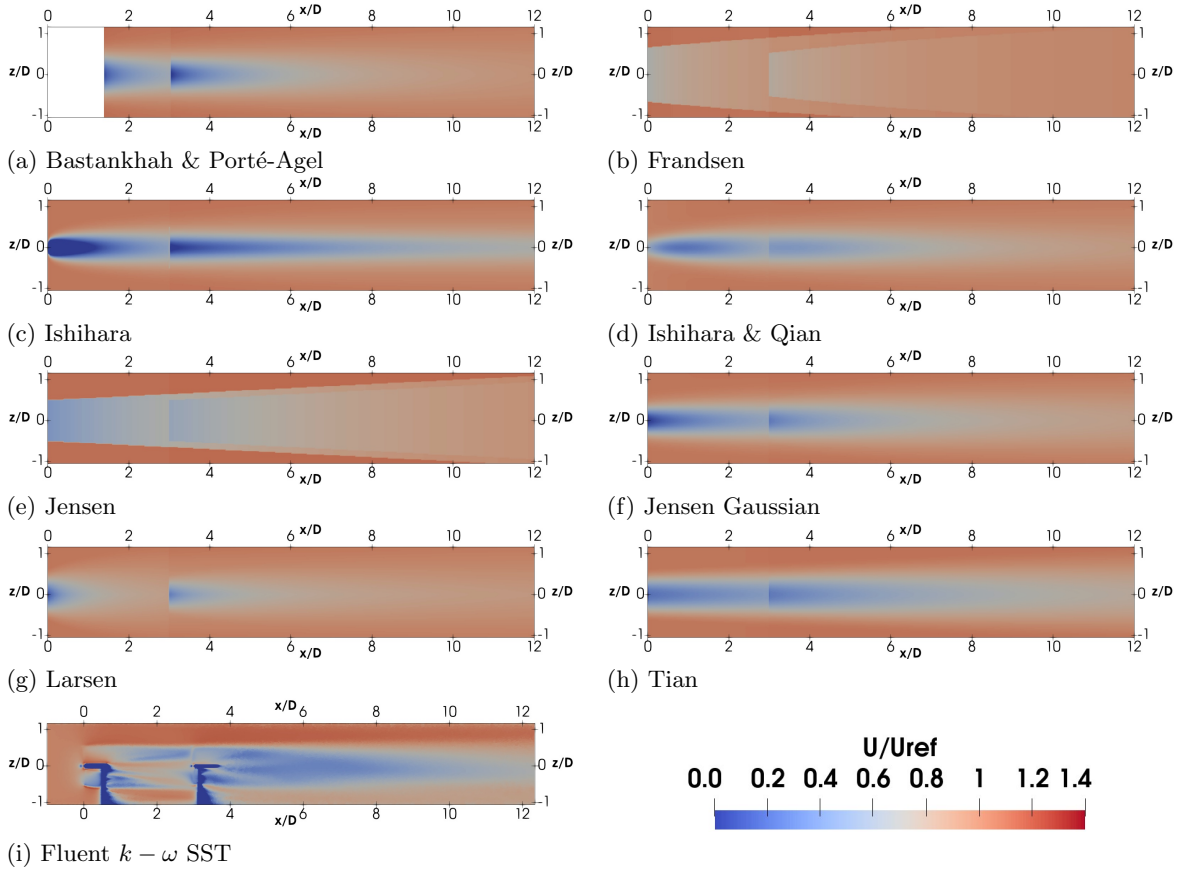

(a) Bastankhah & Porté-Agel (b) Frandsen

(c) Ishihara (d) Ishihara & Qian

(e) Jensen (f) Jensen Gaussian

(g) Larsen (h) Tian

(i) Fluent $k-\omega$ SST

Figure 17: 2D normalized velocity contours on the plane passing hub center (y=0) from the CFD simulation and the wake models for the two-turbine case

are generated with the Niayifar & Porté-Agel superposition model. Although it is not significant, the increase of blockage factor due to increased velocity deficit from the downstream turbine is present in both CFD and wake model results. Since the incoming velocity is non-uniform for the downstream turbine, the wake uniformity differs downstream from the second turbine. The combined effect of the lower velocity incoming at the top part of the rotor and the tower shadow causes a more symmetrical wake downstream of the second turbine. While the CFD simulation predicts a greater velocity deficit behind the downstream turbine than the upstream turbine, almost all the wake models do otherwise. This results in the underestimation of the velocity deficit in Figs. 15 and 16. The reason could be related to the local superposition model. However, one should remark that the global methods result in significant discontinuities at the edge of the downstream wake. Lastly, the Bastankhah model could not determine the velocity distribution near the upstream turbine as in the single-turbine case.

CONCLUSIONS

In this study, the NTNU model wind turbine is simulated in two test cases, a single-turbine case and a two-turbine case where two wind turbines are placed in tandem. The simulation configuration is based on the experimental studies in the literature. The wind tunnel test section, rotor blades, nacelle, and tower are fully resolved in the CFD simulations with RANS equations for a uniform flow with a low and high ambient turbulence intensity. Four different turbulence models ($k-\epsilon$, $k-\omega$, $k-\omega$ SST, and Spalart-Allmaras turbulence models) and two transition models ($k-k_L-\omega$ and Transitional SST models) are used in the simulations. The wake velocity distribution from the CFD simulations is compared with the experimental data from the literature. Moreover, eight

analytical wake models with various complexity are investigated: the Bastankhah & Porté-Agel, Frandsen, Ishihara, Ishihara & Qian, Jensen, Jensen Gaussian, Larsen, and Tian wake models. In addition, linear sum and root sum square superposition methods with local and global velocities for the analytical wake models are compared with each other for the two-turbine case. In the wake models, the blockage factor is applied by applying the conservation of mass with the incompressibility assumption.

It is seen that the double-Gaussian wake shape was observed near the turbine in the experimental results. This shape is mainly due to the tower shadow effect. Since the tower is fully resolved in the CFD simulations, this unsymmetrical behavior is also present in the simulation results. Although both turbulence and transition models overpredict the maximum velocity deficit, almost all of them remarkably predict the wake profile shape close to the experimental results. Nonetheless, simulations with standard $k-\epsilon$, standard $k-\omega$ turbulence models, and $k-k_L-\omega$ transition model could not give the nearly symmetrical Gaussian shape away from the turbine for the single-turbine case. It is seen that the simulations with the Spalart-Allmaras and $k-\omega$ SST turbulence models predict the experimental wake shape the best among the studied models for the single-turbine case. Similarly, the $k-\omega$ SST simulation for the two-turbine case validly determined the wake velocity distribution behind the two-turbine configuration. In addition, all the simulations determined the blockage factor close to the experimental data for the high turbulence intensity case, but they underpredicted it at the low turbulence intensity flow.

Although the analytical wake models are very robust and computationally cheap, they cannot present a valid wake profile close to the turbine since the tower effect is not included in the models. Moreover, the wake models cannot capture the wake decay or the wake expansion in low turbulence levels seen in wind tunnels since the wake models are developed for the wind farm environment. The only exception is the Ishihara wake model which was developed empirically from the wind tunnel experiment data. These behaviors are more apparent in the 2D velocity contours. However, at high turbulence intensity levels, the models are able to predict the wake profile in both spanwise and vertical directions away from the turbine because the velocity profile becomes closer to the Gaussian shape, which is the velocity distribution what most of the wake models predict throughout the solution domain. At the high turbulence intensity level, Tian, Jensen Gaussian, and Ishihara models are the models to predict velocity distributions closest to the experimental and computational results for the single-turbine case. These models are distinct from the other ones from the usage of a wake turbulence intensity relation. Similarly, the Ishihara and Tian models are the most accurate ones for the two-turbine case away from the turbines since they predict both the velocity deficit and the wake expansion quite well. Moreover, the two-turbine case showed that the increased turbulence in the flow due to the rotor/rotor and wake/tower interactions, the velocity profile in both horizontal and vertical direction tends to take a Gaussian shape as the wake model results. Lastly, the CFD simulations show that the wake shape centers below the hub axis in the vertical direction away from the turbine for both cases, probably due to the short wind tunnel height. Nevertheless, the analytical wake models predict that the wake is centered around the hub height. Although the wake models cannot be suitable for understanding the detailed physics in wind turbine wakes, they can be a useful and robust tool for investigating wind farm performance and optimizing the wind farm layout.

The wake model itself is not the only variable that affects the analytical analysis results. Firstly, blockage correction is an important parameter to replicate the flow inside a wind tunnel. The employed method is applied for each wake model and the blockage factor is compared with another factor used in the literature for a similar configuration. The results show that the correction factor changes with the downstream location due to the wake diffusion and depends on which wake model it is applied. Moreover, the employed method gives a factor close to the one used in the literature for most methods. In addition, the wake model results almost match with the experimental data outside the turbine wake diameter, which also verifies the blockage factor method. Secondly, the wake superposition method significantly affects the result for a configuration with multiple turbines. It is seen that the methods with global velocity result in tremendous discontinuities at the edge of

the downstream wake. Moreover, the Lissaman method predicts the maximum velocity deficit too much. Although the Katic et al. method gives a maximum velocity deficit close to the experiments, the overall shape is unacceptable. Thus, the methods with local velocity, Niayifar & Porté-Agel and Voutsinas et al. models, give a valid velocity shape and an acceptable velocity deficit compared to the experimental data.

ACKNOWLEDGMENT

We thank METUWIND, METU Center for Wind Energy at Middle East Technical University, for letting us use their HPC clusters for the CFD simulations of this study.

References

Adaramola, M.S. and Krogstad, P.Å. (2011) *Experimental investigation of wake effects on wind turbine performance*, Renewable Energy, Vol 36, Issue 8, p: 2078-2086, August 2011

Antonini, E.G.A. Romero, D.A. and Amon, C.H. (2019) *Improving CFD wind farm simulations incorporating wind direction uncertainty*, Renewable Energy, Vol 113, p: 1011-1023, April 2019

Antonini, E.G.A. Romero, D.A. and Amon, C.H. (2020) *Optimal design of wind farms in complex terrains using computational fluid dynamics and adjoint methods*, Applied Energy, Vol 261, March 2020

Avial, M. Folch, A. Houzeaux, G. Eguzkitza, B. Prieto, L. and Cabezon, D. (2013) *A Parallel CFD Model for Wind Farms*, Procedia Computer Science, Vol 18, p: 2157-2166, 2013

Barthelmie, R.J. Larsen, G.C. Frandsen, S.T. Folkerts, L. Rados, K. Pryor, S.C. Lange, B. and Schepers, G. (2006) *Comparison of Wake Model Simulations with Offshore Wind Turbine Wake Profiles Measured by Sodar*, Journal of Atmospheric and Oceanic Technology, Vol 23, Issue 7, p: 888–901, July 2006

Bartl, J. Pierella, F. and Sætran, L. (2012) *Wake Measurements Behind an Array of Two Model Wind Turbines*, Energy Procedia, Vol 24, p: 305-312, January 2012

Bartl, J. and Sætran, L. (2016) *Experimental testing of axial induction based control strategies for wake control and wind farm optimization*, Journal of Physics: Conference Series, Vol 753, Issue 3, 2016

Bartl, J. and Sætran, L., (2017) *Blind test comparison of the performance and wake flow between two in-line wind turbines exposed to different turbulent inflow conditions*, Wind Energy Science, Vol 2, p: 55-76, February 2017

Bastankhah, M. and Porté-Agel, F. (2014) *A new analytical model for wind-turbine wakes*, Renewable Energy, Vol 70, p: 116-123, October 2014

Bastankhah, M. Welch, B. Martínez-Tossas, L. King, J. and Fleming, P. (2021) *Analytical solution for the cumulative wake of wind turbines in wind farms*, Journal of Fluid Mechanics, Vol 911, A53, March 2021

Behrouzifar, A. and Darbandi, M. (2019) *An improved actuator disc model for the numerical prediction of the farwake region of a horizontal axis wind turbine and its performance*, Energy Conversion and Management, Vol 185, p: 482-495, April 2019

BP (2021) *bp Statistical Review of World Energy 2021*, London

Castellani, F. Gravdahl, A. Crasto, G. Piccioni, E. and Vignaroli, A. (2013) *A practical approach in the CFD simulation of off-shore wind farms through the actuator disc technique*, Energy Procedia, Vol 35, p: 274-284, 2013

Ceccotti, C. Spiga, A. Bartl, J. and Sætran, L. (2016) *Effect of Upstream Turbine Tip Speed Variations on Downstream Turbine Performance*, Energy Procedia, Vol 94, p: 478-486, September 2016

El-Asha, S. Zhan, L. and Iungo, G.V. (2017) *Quantification of power losses due to wind turbine wake interactions through SCADA, meteorological and wind LiDAR data*, Wind Energy, Vol 20, Issue 11, p: 1823-1839, November 2017.

Ewald, B.F. (1998) *Wind Tunnel Wall Corrections*, Advisory Group for Aerospace Research and Development, AGARD-AG-336, October 1998

Frandsen, S. Barthelmie, R. Pryor, S. Rathmann, O. Larsen, S. Højstrup, J. and Thøgersen, M. (2006) *Analytical modelling of wind speed deficit in large offshore wind farms*, Wind Energy, Vol 9, Issue 1-2, p: 39-53, January-April 2006

Gao, X. Yang, H. and Lu, L. (2016) *Optimization of wind turbine layout position in a wind farm using a newly-developed two-dimensional wake model*, Applied Energy, Vol 174, p: 192-200, July 2016

Ishihara, T. Yamaguchi, A. and Fujino, Y. (2004) *Development of a new wake model based on a wind tunnel experiment*, The University of Tokyo, January 2004

Ishihara, T. and Qian, G. (2018) *A new Gaussian-based analytical wake model for wind turbines considering ambient turbulence intensities and thrust coefficient effects*, Journal of Wind Engineering and Industrial Aerodynamics, Vol 177, p: 275-292, June 2018

Jensen, N.O. (1983) *A note on wind generator interaction*, Risø National Laboratory. Risø-M No. 2411, November 1983

Kaldellis, J.K. Triantafyllou, P. and Stinis, P. (2021) *Critical evaluation of Wind Turbines' analytical wake models*, Renewable and Sustainable Energy Reviews, Vol 144, July 2021

Katic, I. Højstrup, J. Jensen, N.O. (1986) *A Simple Model for Cluster Efficiency*, European Wind Energy Association Conference and Exhibition, Rome, Italy, October 1986

Kollwitz, J. (2016) *Defining the Wake Decay Constant as a Function of Turbulence Intensity to Model Wake Losses in Onshore Wind Farms*, MS Thesis, Uppsala University, October 2016

Krogstad, P.Å. and Eriksen, P.E. (2013) *"Blind test" calculations of the performance and wake development for a model wind turbine*, Renewable Energy, Vol 50, p: 325-333, February 2013

Krogstad, P.Å. and Lund, J.A. (2012) *An experimental and numerical study of the performance of a model turbine*, Wind Energy, Vol 15, Issue 3, p: 443-457, April 2012

Krogstad, P.Å. Sætran, L. and Adaramola, M.S. (2015) *"Blind Test 3" calculations of the performance and wake development behind two in-line and offset model wind turbines*, Journal of Fluids and Structures, Vol 52, p: 65-80, January 2015

Kuo, J.Y.J. Romero, D.A. Beck, J.C. and Amon, C.H. (2016) *Wind farm layout optimization on complex terrains – Integrating a CFD wake model with mixed-integer programming*, Applied Energy, Vol 178, p: 404-414, September 2016

Lantz, E. Hand, M. and Wiser, R. (2012) *The Past and Future Cost of Wind Energy*, 2012 World Renewable Energy Forum, Denver, Colorado, American Solar Energy Society, May 2012

Larsen, G.C. (1988) *A Simple Wake Calculation Procedure*, Risø National Laboratory, Risø-M No. 2760, December 1988

Larsen, G.C. (2009) *A simple stationary semi-analytical wake model*, Risø National Laboratory, Technical University of Denmark, Risø-R-1713, August 2009

Lissaman, P.B.C. (1979) *Energy Effectiveness of Arbitrary Arrays of Wind Turbines*, Journal of Energy, Vol 3, Issue 6, p: 323-328, November-December 1979

Martínez-Tossas, L.A. Churchfield, M.J. and Leonardi, S. (2015) *Large eddy simulations of the flow past wind turbines: actuator line and disk modeling*, Wind Energy, Vol 18, Issue 6, p: 1047-1060, June 2015

Milborrow, D.J. (1980) *The performance of arrays of wind turbines*, Journal of Wind Engineering and Industrial Aerodynamics, Vol 5, Issue 3, p: 403-430, May 1980

Mühle, F., Schottler, J., Bartl, J., Futrzynski, R., Evans, S., Bernini, L., Schito, P., Draper, M., Guggeri, A., Kleusberg, E., Henningson, D.S., Hölling, M., Peinke, J., Adaramola, M.S. and Sætran, L. (2018) *Blind test comparison on the wake behind a yawed wind turbine*, Wind Energy Science, Vol 3, Issue 2, p: 883-903, November 2018

Niayifar, A. and Porté-Agel, F. (2016) *Analytical Modeling of Wind Farms: A New Approach for Power Prediction*, Energies, Vol 9, Issue 9, 741, September 2016

Our World In Data (2021) *Wind energy generation by region*, https://ourworldindata.org/grapher/wind-energy-consumption-by-region

Pierella, F., Krogstad, P.Å. and Sætran, L. (2014) *Blind Test 2 calculations for two in-line model wind turbines where the downstream turbine operates at various rotational speeds*, Renewable Energy, Vol 70, p: 62-77, October 2014

Pierella, F. and Sætran, L. (2017) *Wind tunnel investigation on the effect of the turbine tower on wind turbines wake symmetry*, Wind Energy, Vol 20, Issue 10, p: 1753-1769, October 2017

Polster, M.F. (2017) *Comprehensive comparison of analytical wind turbine wake models with wind tunnel measurements and wake model application on performance modelling of a downstream turbine*, Master Thesis, Norwegian University of Science and Technology, July 2017

Porté-Agel, F. Bastankhah, M. and Shamsoddin, S. (2020) *Wind-Turbine and Wind-Farm Flows: A Review*, Boundary-Layer Meteorology, Vol 174, Issue 1, p: 1-59, January 2020

Richmond, M. Antoniadis, A. Wang, L. Kolios, A. Al-Sanad, S. and Parol, J. (2019) *Evaluation of an offshore wind farm computational fluid dynamics model against operational site data*, Ocean Engineering, Vol 193, December 2019

Ryi, J. Rhee, W. Hwang, U.C. and Choi, J.-S. (2015) *Blockage effect correction for a scaled wind turbine rotor by using wind tunnel test data*, Renewable Energy, Vol 79, p: 227-235, July 2015

Saebzadeh, S. Rezaeiha, A. and Montazeri, H. (2020) *Towards optimal layout design of vertical-axis wind-turbine farms: Double rotor arrangements*, Energy Conversion and Management, Vol 226, December 2020

Sahin, A.D. (2004) *Progress and recent trends in wind energy*, Progress in Energy and Combustion Science, Vol 30, Issue 5, p: 501-543, 2004

Saidur, R. Islam, M.R. Rahim, N.A. and Solangi, K.H. (2010) *A review on global wind energy policy*, Renewable and Sustainable Energy Reviews, Vol 14, Issue 7, p: 1744-1762, September 2010

Schümann, H. Pierella, F. and Sætran, L. (2013) *Experimental Investigation of Wind Turbine Wakes in the Wind Tunnel*, Energy Procedia, Vol 35, p: 285-296, January 2013

Sert, I.O. Cakmakcioglu, S.C. Tugluk, O. and Sezer-Uzol, N. (2014) *The CFD Investigation of Two Non-Aligned Turbines Using Actuator Disk Model and Overset Grids*, Journal of Physics: Conference Series, Vol 524, 2014

Tian, L. Zhu, W. Shen, W. Zhao, N. and Shen, Z. (2015) *Development and validation of a new two-dimensional wake model for wind turbine wakes*, Journal of Wind Engineering and Industrial Aerodynamics, Vol 137, p: 90-99, February 2015

Torres Garcia, E. Aubrun, S. Coupiac, O. Girard, N. and Boquet, M. (2019) *Statistical characteristics of interacting wind turbine wakes from a 7-month LiDAR measurement campaign*, Renewable Energy, Vol 130, p: 1-11, January 2019

Vermeer, L.J. Sørensen, J.N. and Crespo, A. (2003) *Wind turbine wake aerodynamics*, Progress in Aerospace Sciences, Vol 39, Issue 6-7, p: 467-510, August 2003

Voutsinas, S. Rados, K. and Zervos, A. (1990) *On the Analysis of Wake Effects in Wind Parks*, Wind Engineering, Vol 14, Issue 4, p: 204-219, 1990